USM3D-ME Solutions for RANS Test Suite of High-Fidelity CFD Verification Workshop 2024

Mohagna Pandya, Boris Diskin, Craig Hunter, Alaa Elmiligui
NASA Langley Research Center
Andrew Wick, John Hooker
Helden Aerospace

High-Fidelity CFD Verification Workshop 2024
Orlando, Florida
January 6-7, 2024

Outline

- USM3D-ME Overview
- Results for the RANS Test Suite
  - Joukowski Airfoil
  - NACA 0012 Wing in Tunnel
  - CRM High-Lift Wing-Body Configuration
- Summary

USM3D-ME Features for Workshop Solutions

- **Cell-centered, finite-volume, mixed-element, unstructured-grid discretization for Reynolds-averaged Navier-Stokes (RANS) equations**
- **Second-order spatial accuracy**
- **Upwind spatial discretization for meanflow inviscid flux**
  - Cell gradients using Green-Gauss method and nodal solution
  - No gradient limiter
  - Roe's flux-difference splitting scheme
- **Second-order diffusion terms; face-gradients using Mitchell's method**
- **Nonlinear Spalart-Allmaras turbulence model, SA-neg-QCR2000-R (Crot=1)**
  - Discretization of convective term is first order, upwind
  - Modified discretization of diffusion term for improved robustness
- **Hierarchical Adaptive Nonlinear iteration Method (HANIM)**
  - Decoupled meanflow and turbulence-model preconditioners with approximate Jacobian
  - Jacobian-free Newton-Krylov solver for second-order linearization
  - Nonlinear control for solution updates
  - Adaptive CFL
- **Solutions initialized using freestream conditions**
- **Several iterations performed with first-order meanflow discretization before switching to second order**

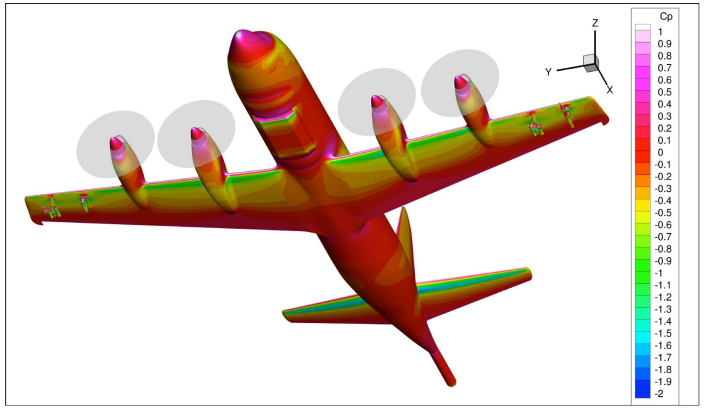

P3-Orion
Courtesy: Craig Hunter (NASA LaRC)

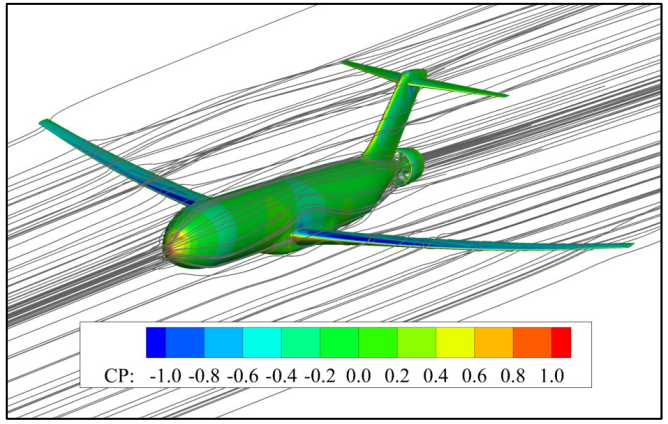

CRM-TCT Configuration
Courtesy: Michael Bozeman (NASA LaRC)

USM3D-ME Other Key Features
Building on Legacy USM3D Flow Solver

- **Standard and specialized boundary conditions**
- **Force-term approach for propellers and other applications**
- **Time integration**
  - Second-order BDF2 for temporal accuracy
- **Rigid-body 6-DoF motion support**
- **Parallelized using MPI paradigm; excellent scalability**
- **Internal extraction of solution functions (e.g., pressure signatures)**
- **Extensive verification through benchmark flow solutions and participation in community workshops**
- **20–30x increase in solution throughput relative to legacy USM3D on complex configuration**
- **Leveraged capabilities**
  - Integration with NASA CDISC for knowledge-based design
  - Integration with NASA grid adaptation tool REFINE

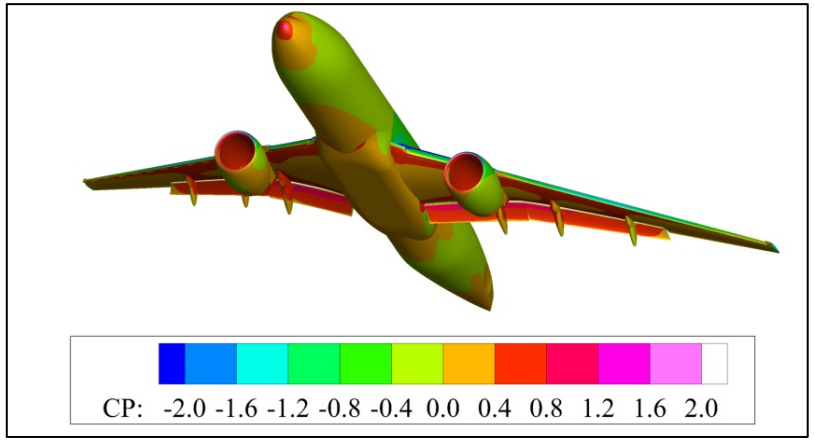

CRM-HL Configuration (HLPW4)
Courtesy: Michael Bozeman(NASA LaRC)

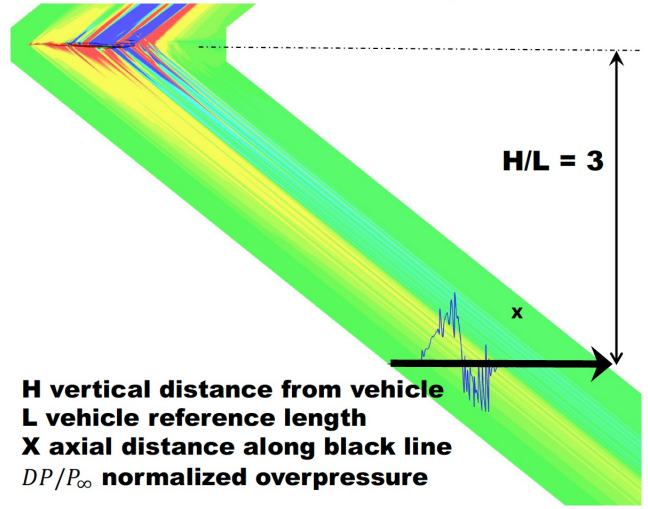

Generic Supersonic Transport
Courtesy: Alaa Elmiligui (NASA LaRC)

AIAA 2013-2541, *AIAA Journal*, 54(9) 2016, *AIAA Journal*, 55(10) 2017, AIAA 2019-2333, *AIAA Journal*, 59(8) 2021, *AIAA Journal*, 59(11) 2021

Joukowski Airfoil

$M_\infty = 0.15$, $\alpha = 0^o$, $Re_c = 6\times10^6$

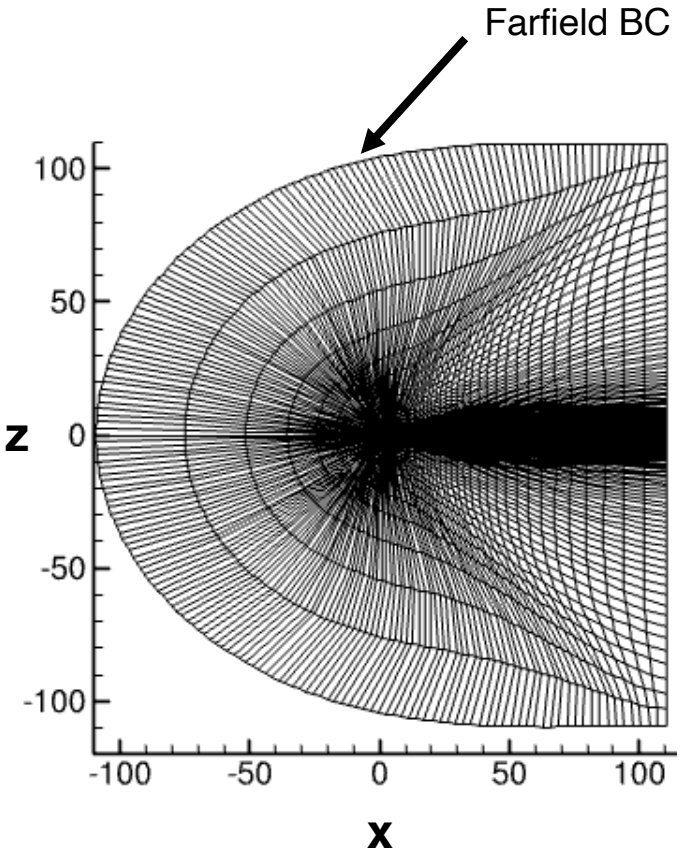

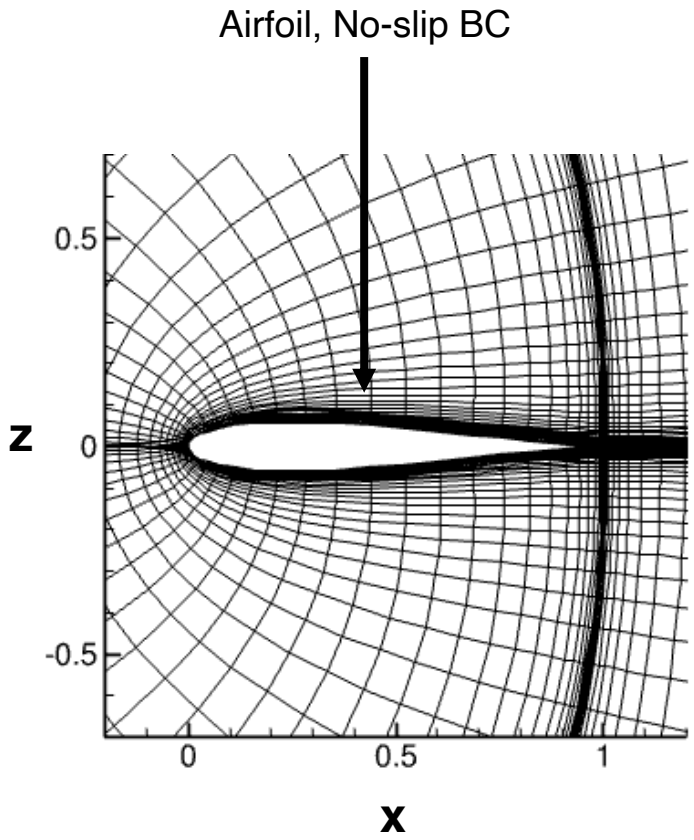

MIT Grid Family

Grid Identifier	Nodes	Cells
L0	1.6K	0.8K
L1	6.3K	3.1K
L2	25.0K	12.3K
L3	99.1K	49.2K
L4	394.8K	196.6K
L5	1.6M	786.4K

Joukowski Airfoil
Iterative and Grid Convergence

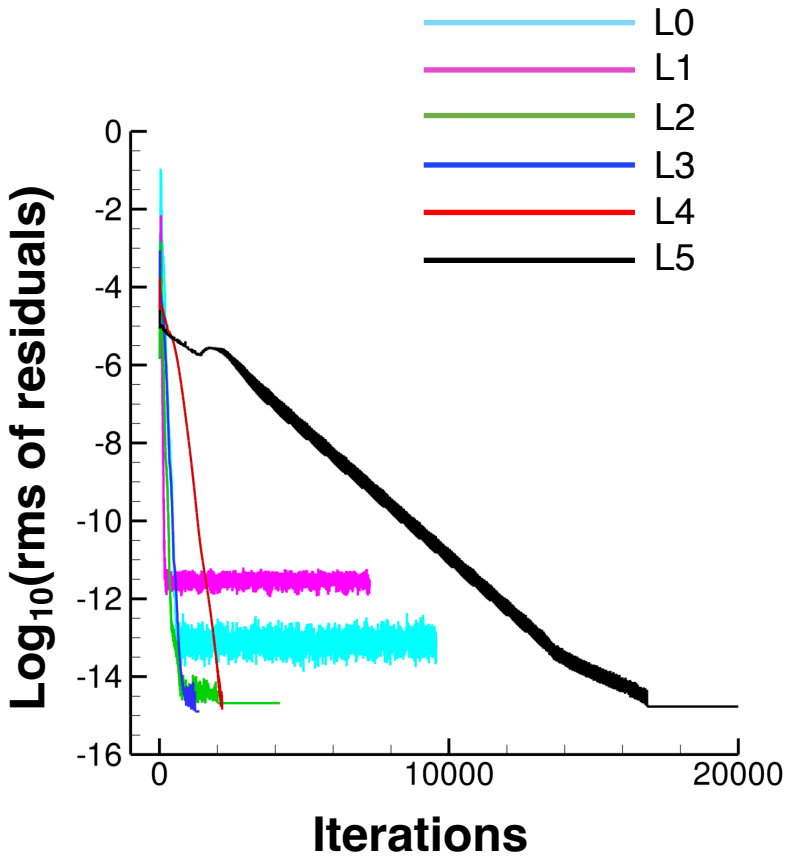

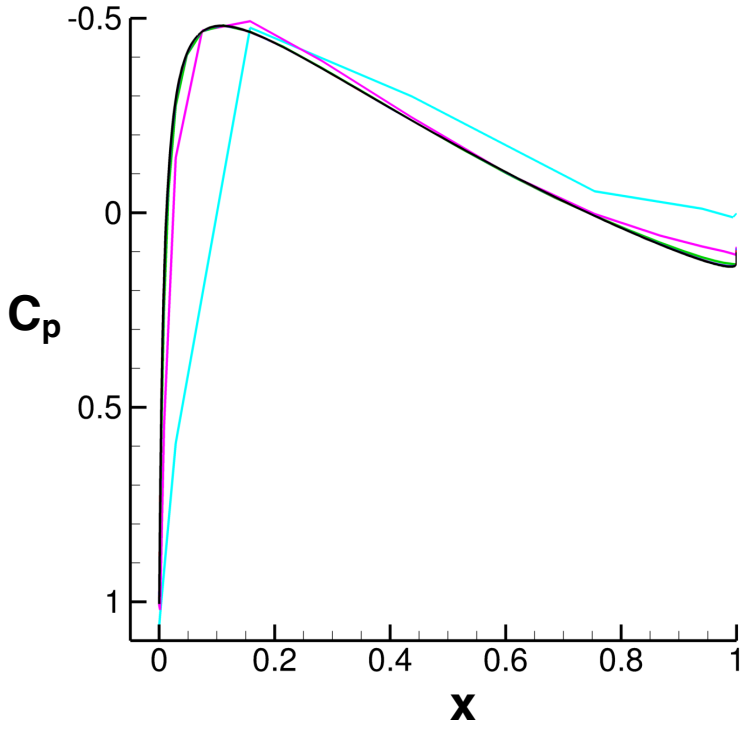

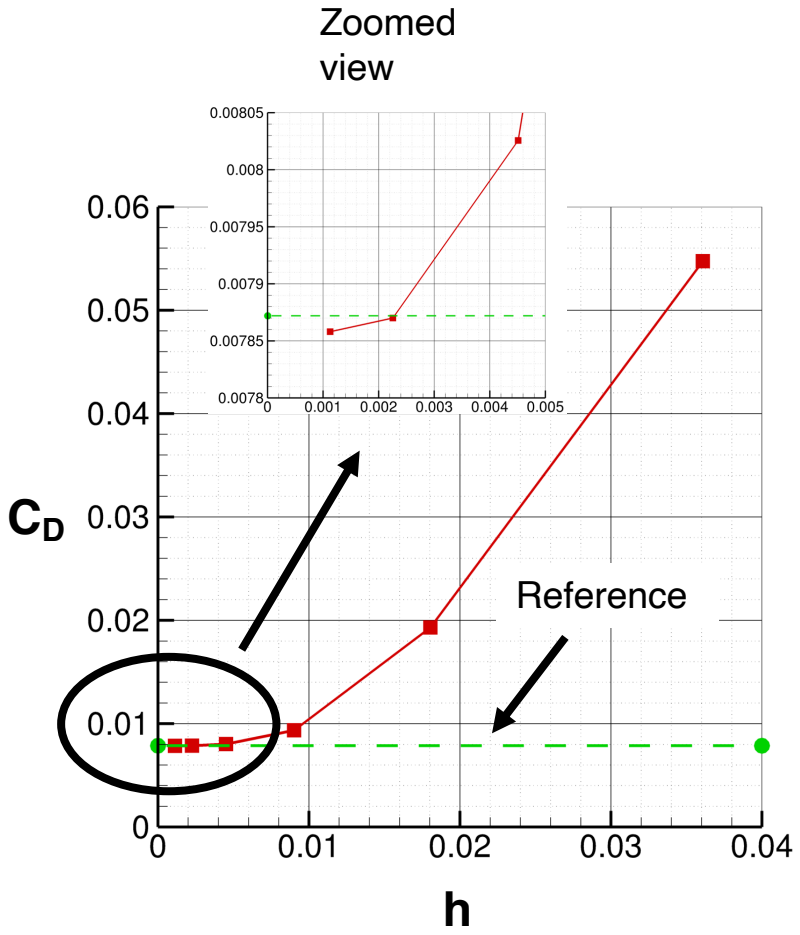

- Meanflow and SA model residuals are combined
- First-order iterations are not shown in the plots
- Reference is fourth-order MIT FEM solution on finest adaptive grid

NACA 0012 Wing in Tunnel

$M_\infty = 0.2$, $\alpha = 0^o$, $Re_c = 4.6 \times 10^6$

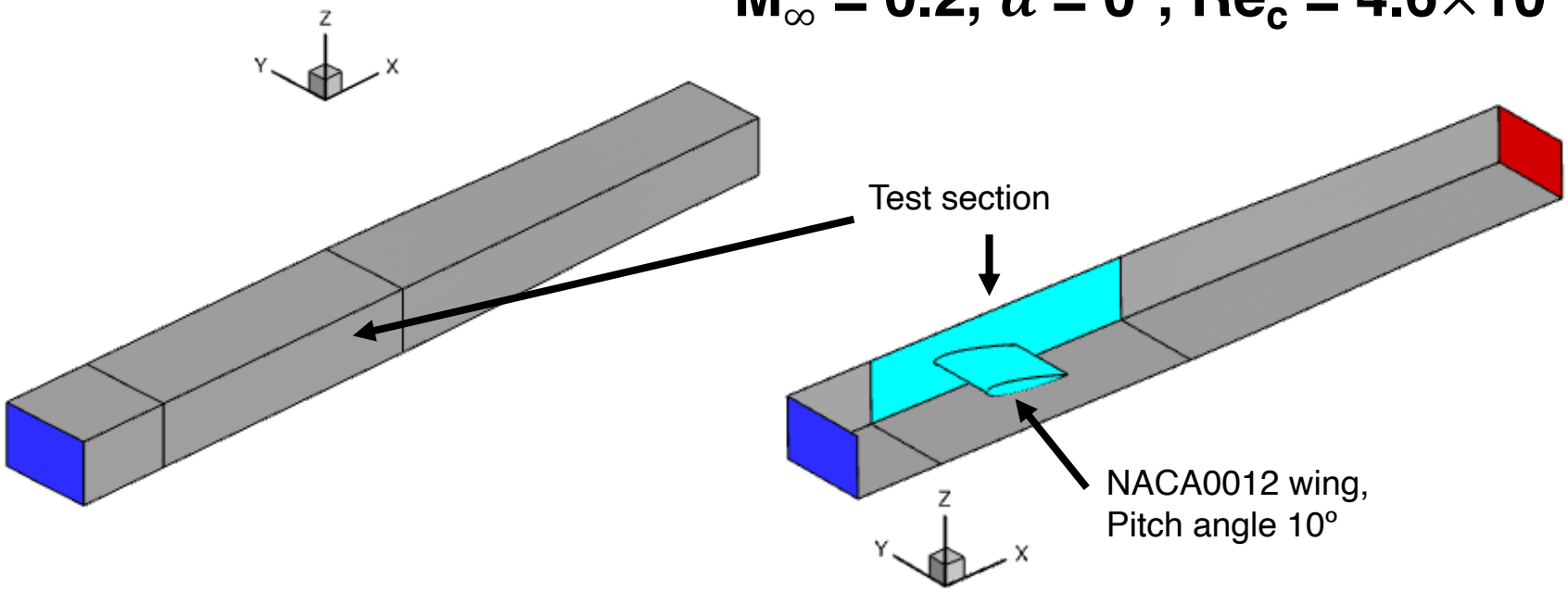

Inflow BC

Outflow BC

Slip wall BC

No-Slip wall BC

HeldenMesh Family

Grid Identifier	Nodes	Cells
A1	40.6K	162.1K
B1	166.6K	520.8K
C1	990.9K	2.5M
D1	6.8M	15.7M
E1	51.1M	111.2M

Pointwise Family, Version 4

Grid Identifier	Nodes	Cells
1.5	3.3M	8.2M
2.0	6.8M	17.1M
3.0	19.5M	50.7M
4.0	42.3M	112.9M
5.0	78.0M	212.1M

MIT Solution-Adapted Grids

Grid Identifier	Nodes	Cells
40K	36.7K	195.2K
80K	72.4K	395.7K
160K	142.5K	794.5K
320K	280.6K	1.6M
640K	566.5K	3.2M

NACA 0012 Wing in Tunnel
Iterative and Grid Convergence

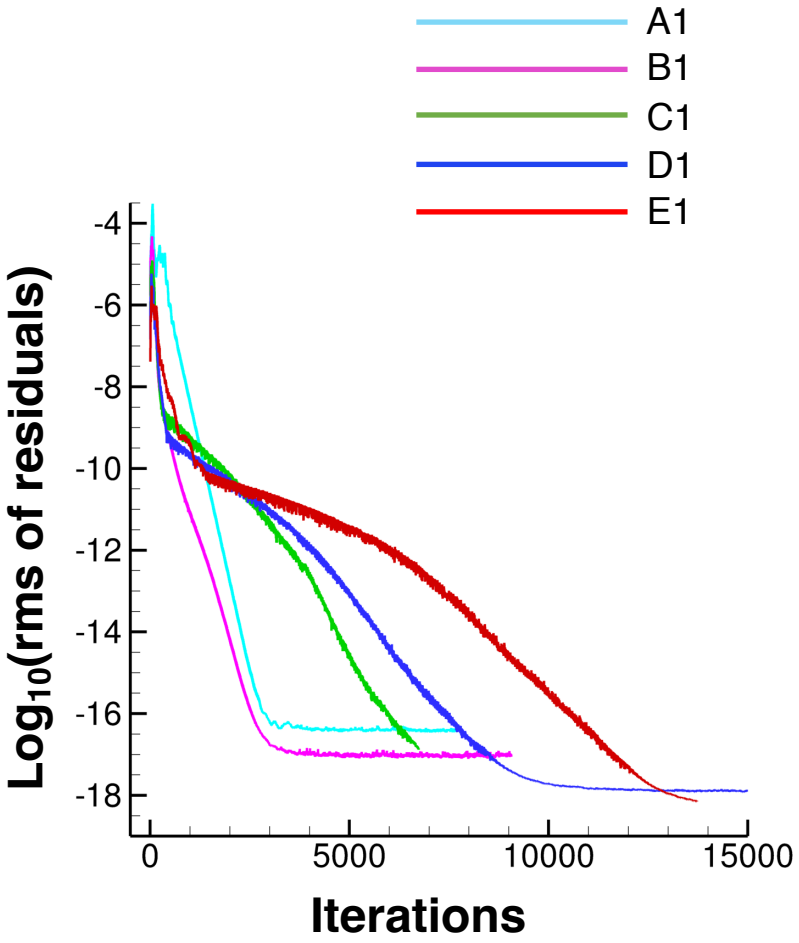

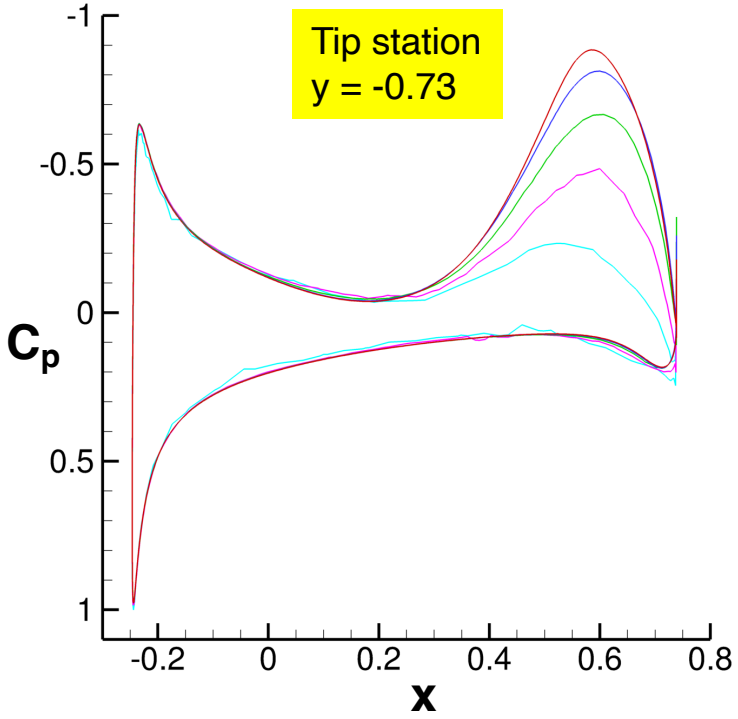

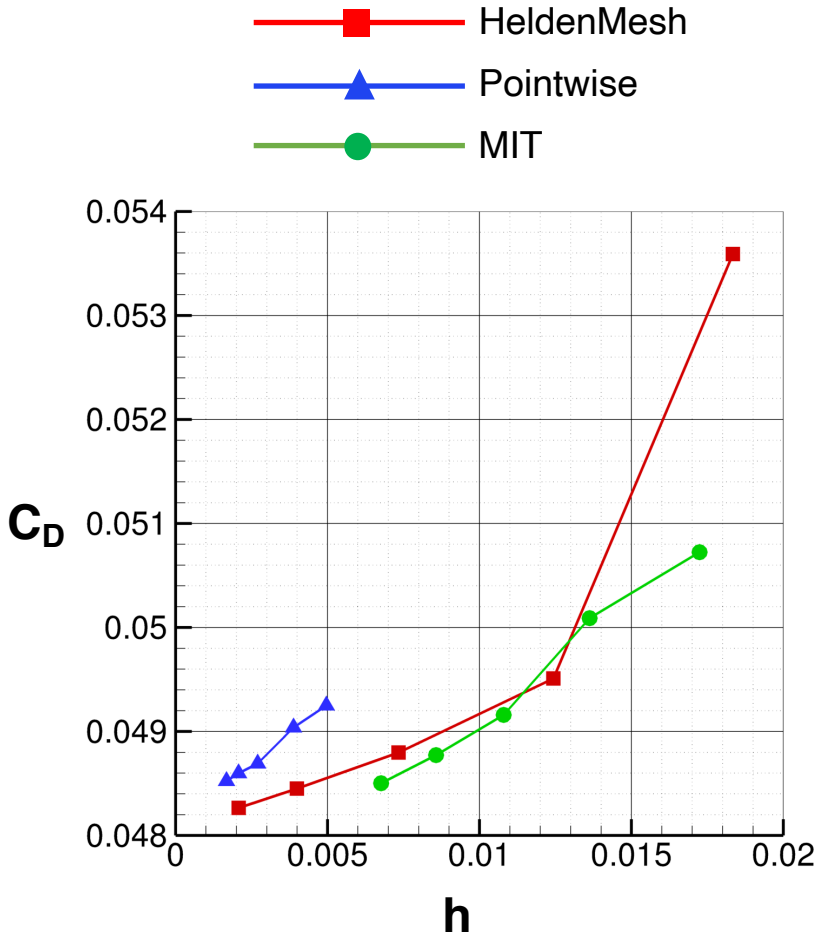

- Residual and Cp plots for HeldenMesh grid family
- Meanflow and SA model residuals are combined
- First-order iterations are not shown in the plots

NACA 0012 Wing in Tunnel

Effect of Rotation Correction (R), HeldenMesh Grid E1, x = 0.805 plane

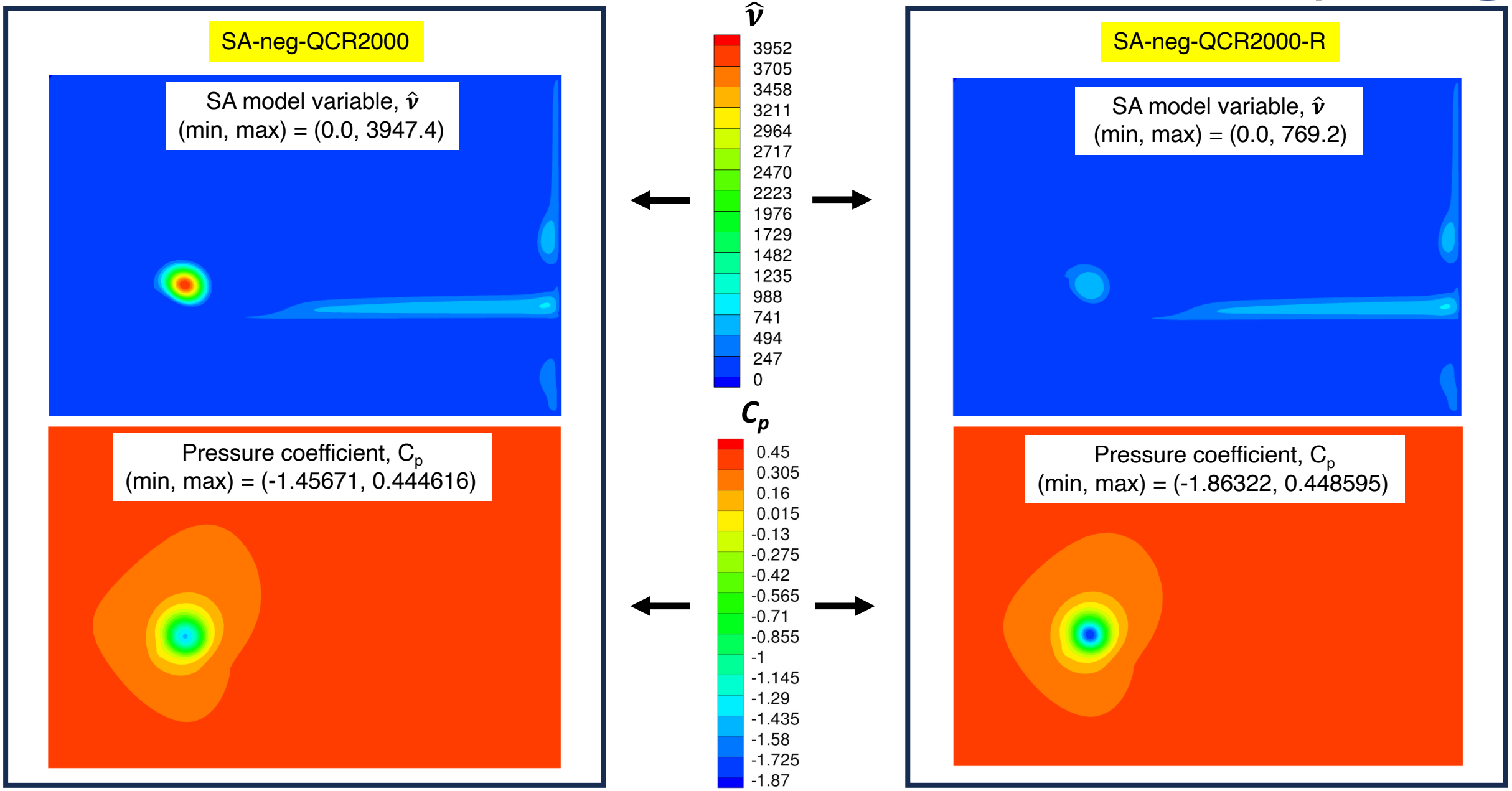

CRM High-Lift Wing-Body Configuration

$M_\infty = 0.2$, $\alpha = 11°$, $Re_c = 5.6 \times 10^6$

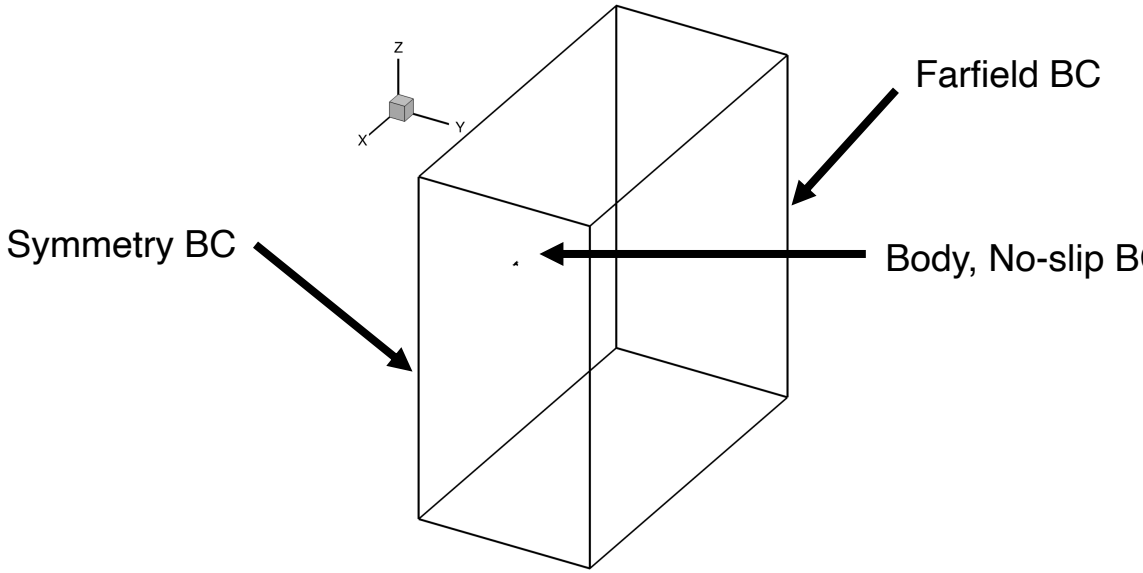

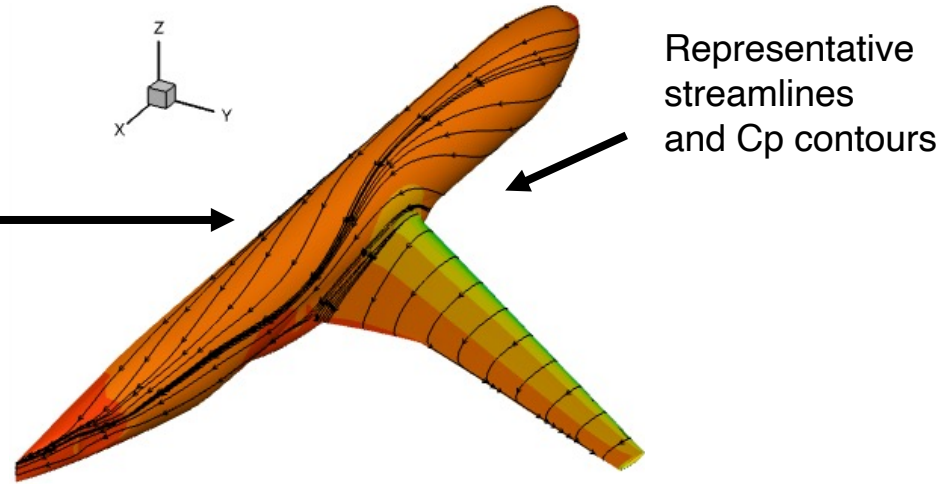

HeldenMesh R.05 Family

Grid Identifier	Nodes	Cells
C	864.0K	2.6M
M	5.8M	17.8M
F	42.9M	131.0M
R	331.2M	1.01B

HeldenMesh R.07 Family

Grid Identifier	Nodes	Cells
Coarse	5.0M	12.0M
Medium	13.4M	31.2M
Fine	38.9M	87.1M
XFine	105.6M	232.4M
UFine	191.0M	415.1M

CRM High-Lift Wing-Body Configuration
Iterative and Grid Convergence

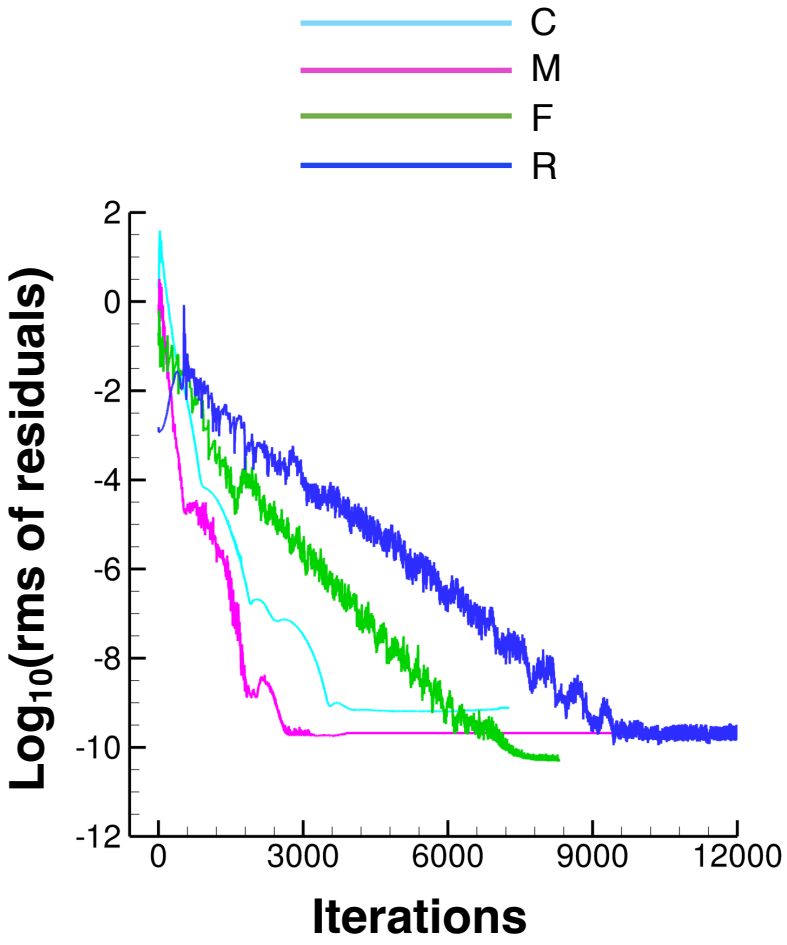

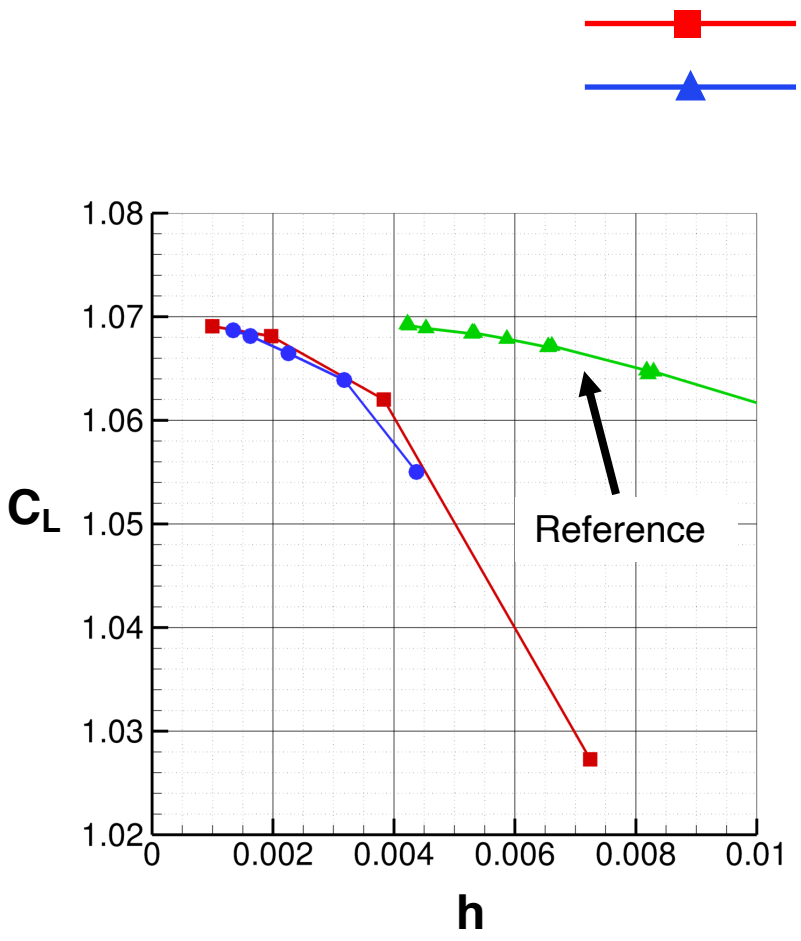

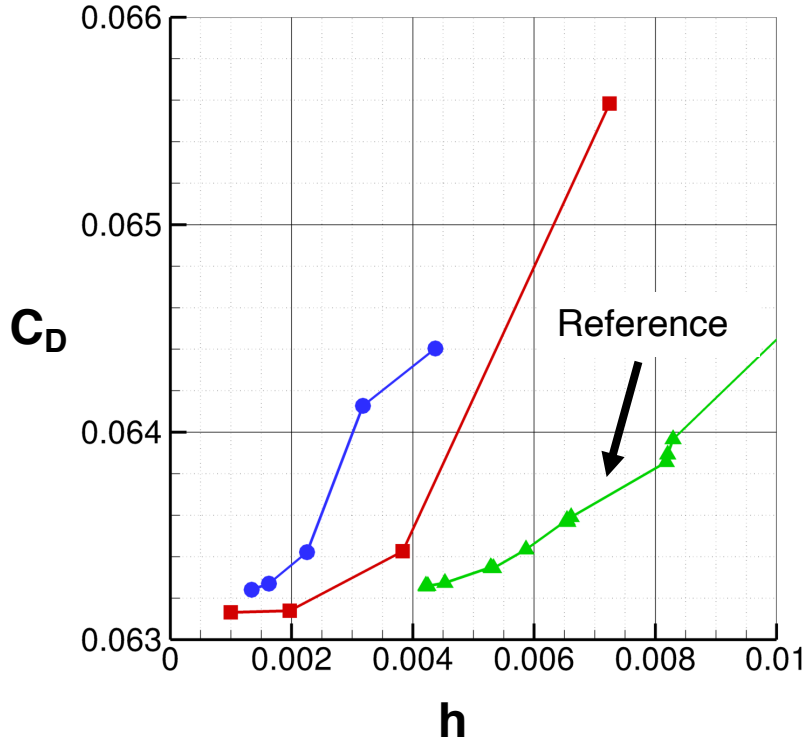

- Residual plot for HeldenMesh R.05 grid family
- Meanflow and SA model residuals are combined
- First-order iterations are not shown in the plots
- Reference is Boeing FEM solution on adaptive grids

Summary

- **USM3D-ME solutions computed using SA-neg-QCR2000-R (C_{rot} = 1) turbulence model**
  - Joukowski airfoil
  - NACA 0012 wing in tunnel
  - CRM High-Lift Wing-Body Configuration
- **Solutions on different grid families**
  - Structured, unstructured mixed-element, and adaptive tetrahedral grids
- **Machine-zero residuals achieved on all cases and grids**
- **Satisfactory grid convergence observed for all cases**
- **Joukowski airfoil**
  - Difference in C_D on two finest grids is 0.12 count
- **NACA 0012 wing in tunnel**
  - Difference in C_D between finest grids within two families is 2.57 count
  - Effect of rotation correction (R) illustrated
- **CRM High-Lift Wing-Body Configuration**
  - Difference in C_D between finest grids within two families is 1.09 count
  - Difference in C_L between finest grids within two families is 0.04%

Acknowledgments

- Work reported herein is funded by NASA ARMD Transformational Tools and Technologies (TTT) project
- Computations were conducted on NAS Pleiades supercomputing facility and LaRC k cluster
- HeldenMesh development supported under NASA SBIRs: 80NSSC18C0078, 80NSSC20C0094, 80NSSC22CA236, and 80NSSC23CA102